Guided-Wave Photonics

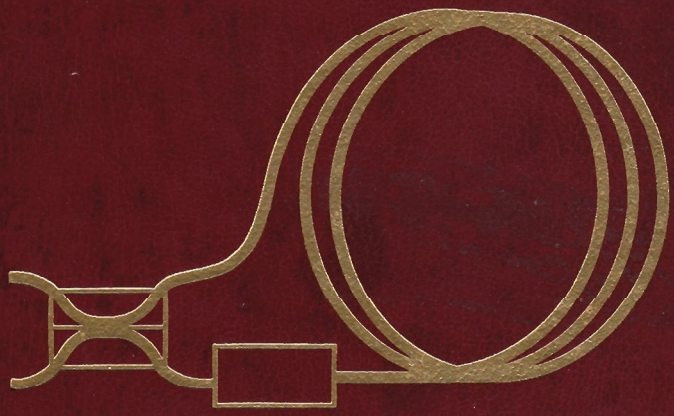

BUCKMAN

Text Typeface: Times Roman
Compositor: Tapsco, Inc.
Senior Acquisitions Editor: Barbara Gingery
Assistant Editor: Laura Shur
Managing Editor: Carol Field
Project Editor: Janet B. Nuciforo
Copy Editor: Merry Post
Manager of Art and Design: Carol Bleistine
Art Director: Doris Bruey
Text Designer: Rita Naughton
Cover Designer: Lawrence R. Didona
Text Artwork: Vantage Art
Production Manager: Charlene Squibb
Director of EDP: Tim Frelick

Printed in the United States of America

GUIDED-WAVE PHOTONICS

ISBN 0-03-033354-7

Library of Congress Catalog Card Number: 91-050888

1234 039 987654321

such as the one shown in Figure 1.2. This allows a degree of parallel processing that is exploited in each of the devices described below.

7.3.2 Guided-Wave Real-Time Spectrum Analyzer (13)

With electronic computation, obtaining the power spectrum of a received signal requires sampling a large number of points and then calculating a different integral for each frequency at which a value for the power spectrum is desired. Since each calculation occurs in sequence in a conventional electronic computer, the entire spectrum of a wideband signal takes a long time to generate. The device shown in Figure 7.13 generates the power spectrum much faster. Light from a CW laser is butt-coupled into the slab waveguide, before entering the two-dimensional lens, L1, which collimates the guided wave into a "beam" in the slab, with a width W. This beam interacts with the surface acoustic wave produced at the transducer. The geometry of this interaction is the same as that in Figure 7.10(a). Neglecting any Doppler shift in the light frequency in Equation (7-71) requires that

$$\omega_i = \omega_D \tag{7-76}$$

which means that the incident and diffracted modes will differ only in direction and not in propagation constant, or

$$|\beta_i| = |\beta_D| \tag{7-77}$$

in Equation (7-70). The vector momentum conservation diagram in Figure 7.10(b) is thus an isosceles triangle, with the diffraction angle θ given by

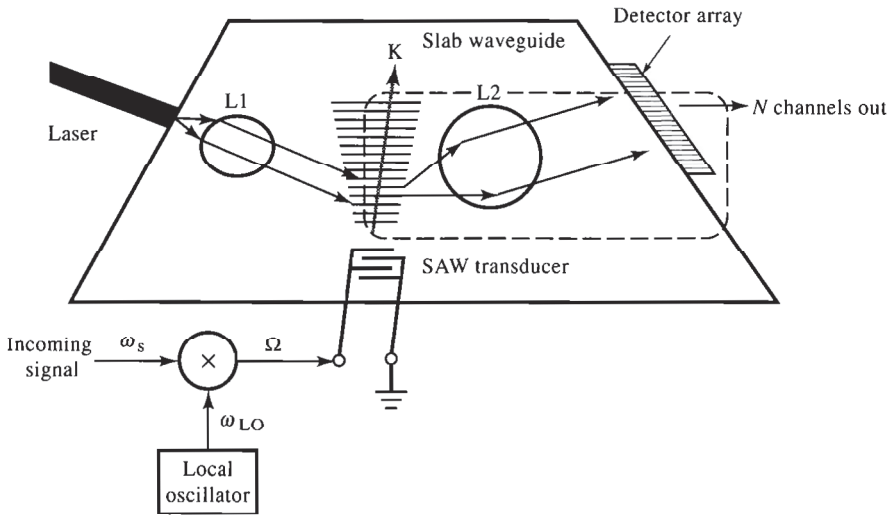

Figure 7.13 Schematic of a guided-wave real time spectrum analyzer.

$$\theta = \sin^{-1}\left[\frac{|\mathbf{K}|}{2|\beta|}\right] \tag{7-78}$$

In view of Equation (7-77), the i and D subscripts have been dropped in Equation (7-78). The surface acoustic wave propagation velocity is constant over a wide acoustic frequency range, and obeys the relation

$$v_{SAW} = \frac{\Omega}{|\mathbf{K}|} \tag{7-79}$$

which is just the general wave property (Eq. 1-11), written for the surface acoustic wave. Solving Equation (7-79) for $|\mathbf{K}|$ and substituting the result into Equation (7-78) produces the desired relation between acoustic frequency and diffraction angle

$$\theta = \sin^{-1}\left[\frac{\Omega}{2v_{SAW}|\beta|}\right] \tag{7-80}$$

Before being applied to the SAW transducer in Figure 7.12, the incoming signal is mixed with a single-frequency sinusoid at ω_{LO} from the local oscillator, so that the SAW frequency is related to the incoming signal frequency, ω_s, by

$$\Omega = \omega_{LO} + \omega_s \tag{7-81}$$

Actually, the incoming signal consists of multiple components at different ω_s, yielding diffracted guided modes at multiple values of θ. The second waveguide lens, L2, collimates light diffracted into a particular direction onto a particular detector in the array at the right side of the slab waveguide in Figure 7.13. Each signal component at a different ω_s corresponds to a different diffraction angle calculated by substituting Equation (7-81) into Equation (7-80). Assuming the guided mode power diffracted into any θ is proportional to the signal power at the corresponding ω_s, this device yields a set of currents from each detector in the array that is proportional to the signal power in a narrow frequency band centered at ω_s.

To see this more clearly, consider the region enclosed by the dashed line in Figure 7.13, magnified to yield Figure 7.14. Let the center frequency of the incoming signal be ω_c, and the diffraction angle corresponding to ω_c be the angle θ_c shown in Figure 7.14. If the lens L2 is situated a focal length, f, away from the interaction region, all diffracted energy in the angular range $\Delta\theta$ arrives at one detector of width L. For small θ_1, the range of angles incident on a single detector of width L is given by

$$\Delta\theta = \frac{L}{f} \tag{7-82}$$

Differentiating Equation (7-80) with respect to Ω, and using Equation (7-81) gives

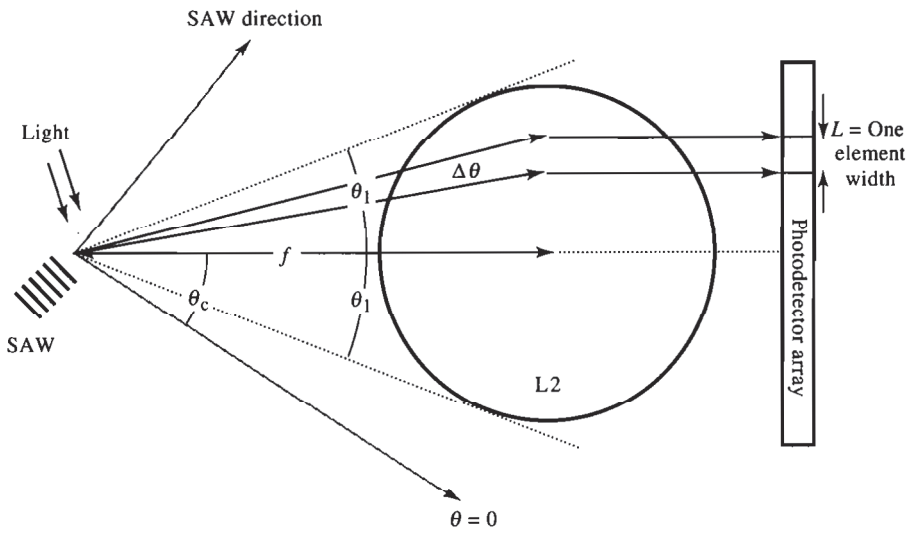

Figure 7.14 Diffraction and focusing on the detector array in the guided-wave real time spectrum analyzer.

$$\frac{d\theta}{d\Omega} = \frac{d\theta}{d\omega_s} = \frac{1}{2v_{SAW}|\beta|}\left\{1 - \left[\frac{\omega_{LO} + \omega_s}{2v_{SAW}|\beta|}\right]^2\right\}^{-1/2} \tag{7-83}$$

Solving Equation (7-83) for $d\omega_s$ and substituting Equation (7-82) for $\Delta\theta$ gives the channel bandwidth associated with each detector in the array as

$$d\omega_s = 2v_{SAW}|\beta|\left\{1 - \left[\frac{\omega_{LO} + \omega_s}{2v_{SAW}|\beta|}\right]^2\right\}^{1/2}\frac{L}{f} \tag{7-84}$$

If the array contains N detectors, the device in Figure 7.13 computes a power spectrum of the incoming signal over the range of ω_s corresponding to the range of diffracted angles

$$\theta_c - \theta_1 < \theta < \theta_c + \theta_1 \tag{7-85}$$

with N-point resolution along the frequency axis. This power spectrum is computed in the time it takes for the light in the waveguide to propagate from the laser to the detector array. Conventional methods for computing a power spectrum require many successive summations and/or integrations, each of which can involve considerable computation time.

7.3.3 The Integrated Optic Spatial Light Modulator (IOSLM)

Like the real-time spectrum analyzer, the integrated optic spatial light modulator (abbreviated IOSLM) operates on the principle of diffraction of a guided mode

by a controllable g
electrical signal. L
structure like the
of the electro-optic
linear array of gra
in Figure 7.15. Th
the grating period,
in the IOSLM is
Figure 7.15. In th
guided mode wav

Each cell of t
modeled in Sectio
electro-optic mod
assembled into a
of each cell must
from that cell do

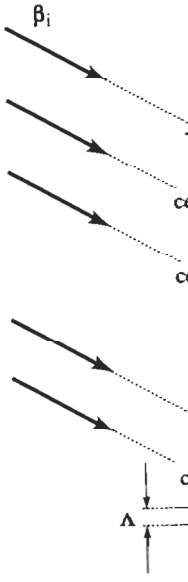

Figure 7.15 Geo
devices are show
second.

by a controllable grating structure formed in a slab waveguide in response to an electrical signal. Instead of a surface acoustic wave, an interdigital electrode structure like the one in Figure 7.9 forms the grating in the IOSLM, by means of the electro-optic effect described in Section 7.2.1. The IOSLM consists of a linear array of grating modulators based on Figure 7.9 with a geometry shown in Figure 7.15. The angle of diffraction is not adjustable in the IOSLM, since the grating period, Λ, is fixed when the device is fabricated. However, each cell in the IOSLM is individually addressable using the appropriate drive line in Figure 7.15. In this way, the intensity in each section of the broad, incident guided mode wavefront is modulated individually.

Each cell of the IOSLM is an electro-optic Bragg modulator like the one modeled in Section 7.2.1 and can be evaluated using the criteria developed for electro-optic modulators earlier in this chapter. When an array of such cells is assembled into an IOSLM, some additional constraints apply. The width, W, of each cell must be large enough so that the transmitted and diffracted beams from that cell do not spread out appreciably from diffraction over the propagation

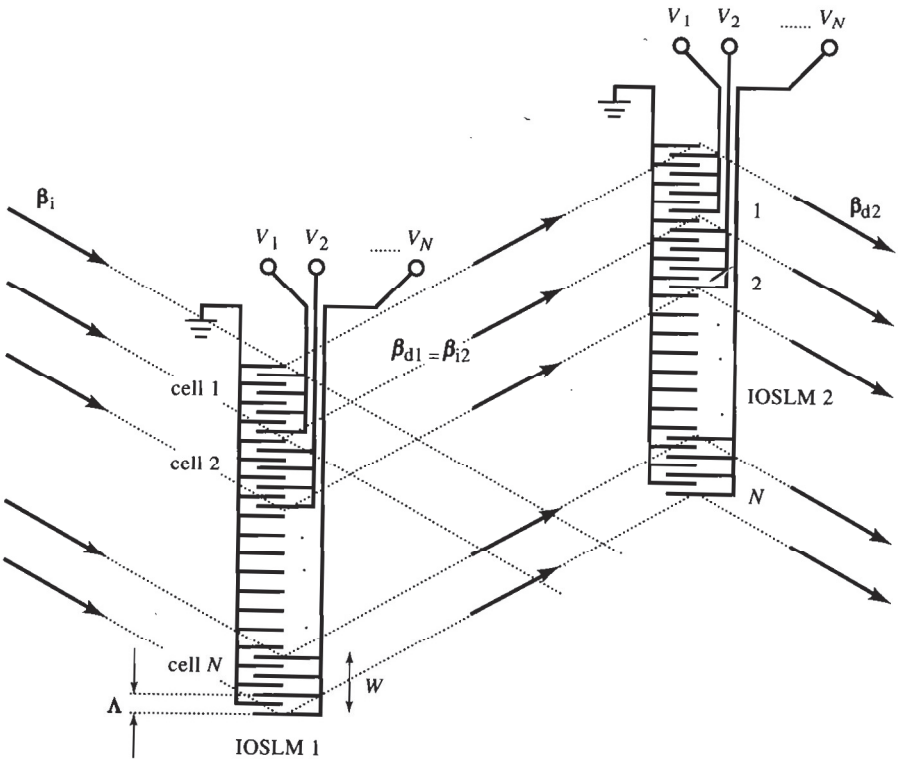

Figure 7.15 Geometry for an integrated optic spatial light modulator (IOSLM). Two devices are shown, with the diffracted output from the first serving as the input for the second.

instances to the next elements (detectors or other devices) in the system. Thus W should be much larger than the wavelength of the guided mode in the slab.

Two or more IOSLMs placed in optical series with each other, as shown in Figure 7.15, are capable of a number of computational functions. For example, suppose that no light is diffracted by a cell with no applied voltage and that, at an applied voltage V_{max}, the cell diffracts essentially all of the guided mode incident on it. Some diffraction is present for all applied cell voltages in the range

$$0 < V_c < V_{max} \tag{7-86}$$

Let the cell voltages in modulator 1 in Figure 7.15 be chosen to represent N sampled values of a function $f(x)$, as represented in Figure 7.16. Since the diffracted power from any cell is always positive, $f(x)$ must be restricted to positive values only. For scaling purposes, let the maximum value of $f(x)$ be one. As pointed out in Section 7.2.1, the diffracted intensity is not linear with V_c, but instead proportional to $\sin^2(aV_c)$, where a is a constant dependent on electrode geometry and waveguide properties. Therefore, the diffracted power from each cell will be linear with $f(x)$ if the voltage corresponding to the value of f is

$$V = \frac{1}{a}\sin^{-1} f \tag{7-87}$$

Returning again to Figure 7.15, suppose that a second function $g(x)$ is sampled using the same procedure employed with $f(x)$ and the resulting voltages placed on the cells of the second IOSLM. From Figure 7.15, the diffracted output from the Mth cell of the second IOSLM is clearly the product of $f(M)g(M)$. Thus, the intensity profile of the diffracted output of the second IOSLM is a sampled product of $f(x)g(x)$.

The device in Figure 7.15 extracts an analog product of two positive functions very rapidly by operating on all the samples simultaneously. As such, it is another

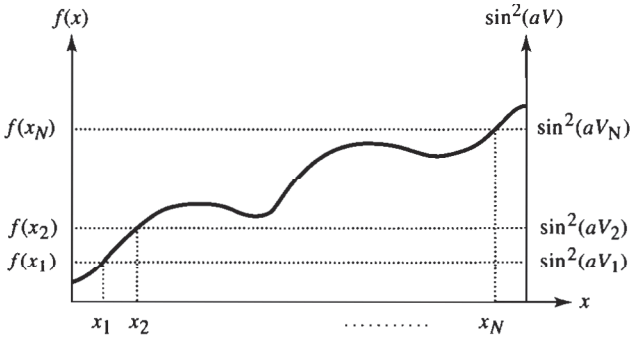

Figure 7.16 Representing the sampled values of a positive function $f(x)$ by a series of voltage levels.

example of the capability
ations. Since the sampled
IOSLM electronically usi
of shifted functions, such
Figure 7.15, a shift would
of $f(x)$ by +P cells just m
that in cell M. In convoluti
is integrated over the dom
IOSLM outputs is readily
Figure 7.17. The lens perfo
from all cells of the IOS
$h(x)$, the integration is eq

where N is the number of

In the IOSLM mode
voltage levels. The values
for $f(x)$ of zero or one o
operations on the zeroes
in Figure 7.16, in paralle

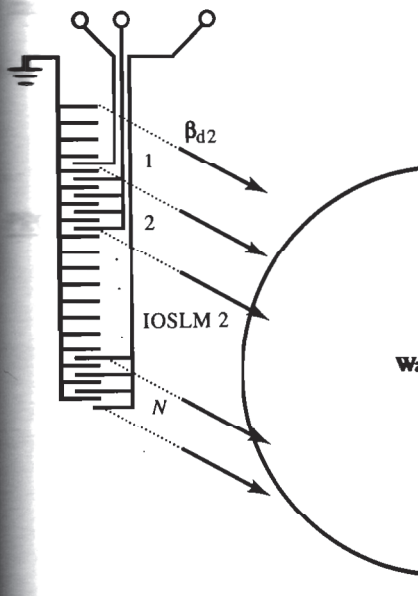

Figure 7.17 Integration across the front
detector.

example of the capability optical devices have for parallel computational operations. Since the sampled values of $f(x)$ and $g(x)$ can be shifted across each IOSLM electronically using shift registers, operations requiring multiplication of shifted functions, such as correlation and convolution, are also possible. In Figure 7.15, a shift would just reassign cell values so that, for example, a shift of $f(x)$ by +P cells just means that the value of V_c in cell M + P is replaced by that in cell M. In convolution and correlation, the product of two shifted functions is integrated over the domain, x, of the functions of interest. This integration of IOSLM outputs is readily accomplished with a guided-wave lens, as shown in Figure 7.17. The lens performs the integration in Figure 7.17 by converging light from all cells of the IOSLM onto a single detector. For a sampled function, $h(x)$, the integration is equivalent to summing the outputs from all cells, or

$$\int h(x)\,dx = \sum_{q=1}^{N} h_q \tag{7-88}$$

where N is the number of samples or cells.

In the IOSLM model developed above, the V_c are assumed to be analog voltage levels. The values of V_c can also be restricted to correspond with values for $f(x)$ of zero or one only. In this case, the IOSLM performs bit-level logic operations on the zeroes or ones in each corresponding cell of the two IOSLMs in Figure 7.16, in parallel. For example, the diffracted output of the second

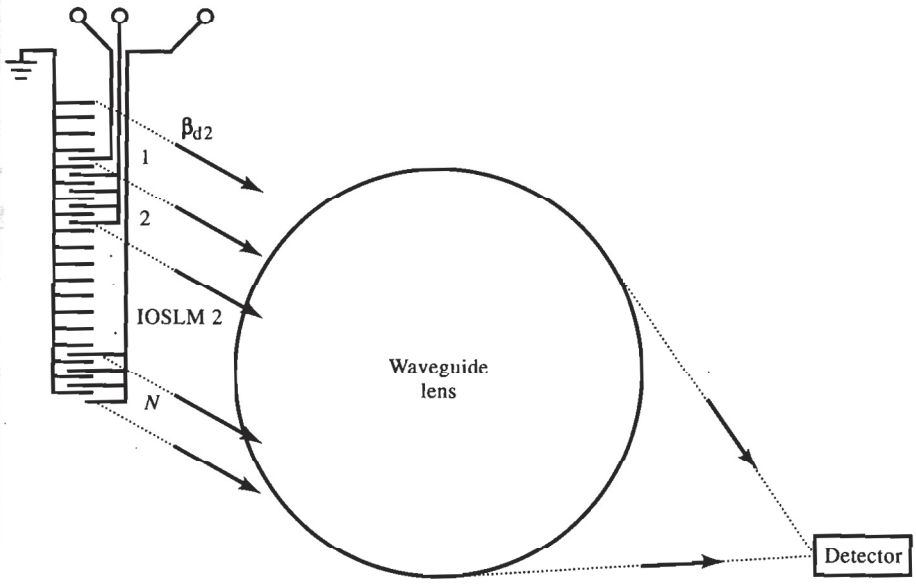

Figure 7.17 Integration across the front of an IOSLM using a lens and a single detector.

IOSLM is the result of a bit-by-bit logical AND of the strings of zeros and ones in the two IOSLMs.

7.3.4 Analog-to-Digital Conversion with Guided-Wave Optics (14)

The final example of guided-wave information subsystems that exploit the inherent parallelism of optical processing is the analog-to-digital converter. Its conceptual similarity to the IOSLM in the preceding section will be immediately apparent. The analog-to-digital converter described here is a parallel arrangement of electro-optic switches similar to the one in Figure 7.6. Each switch corresponds to one bit of precision in the A-to-D conversion. The analog voltage to be converted is applied simultaneously to all electro-optic switches in the converter. An example with four-bit precision is shown in Figure 7.18. The electrode length for the most-significant bit (MSB) is chosen such that the maximum voltage to be converted can cause a π phase shift in the switch for that bit. Moving down the structure of Figure 7.18, the electrode length doubles with each decrease in bit significance so that, for the 4-bit example shown, the electrode length of the least significant bit (LSB) is eight times that of the MSB. The discriminators (DISCR) that follow the detectors convert all detector outputs to discriminator outputs, V_D, which are logical zeros or ones according to the following rule:

$$V_D = \begin{cases} 0 & ; \text{if} \quad 0 < P < P_{max}/2 \\ 1 & ; \text{if} \quad P_{max}/2 < P_{max} \end{cases} \tag{7-89}$$

where P is the optical power incident on a detector and P_{max} is the maximum optical power that can be transmitted through the switch.

Figure 7.19 illustrates the operation of the device in Figure 7.18 as an analog-

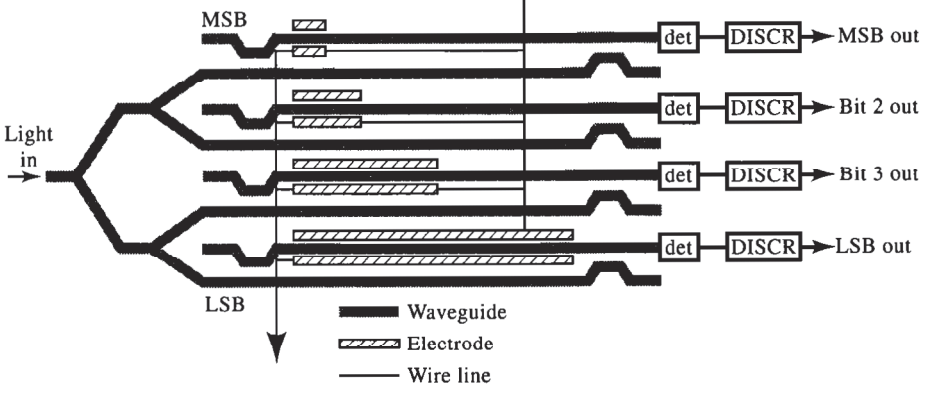

Figure 7.18 A 4-bit guided-wave optical analog to digital converter based on four parallel Mach–Zehnder electro-optic switches.

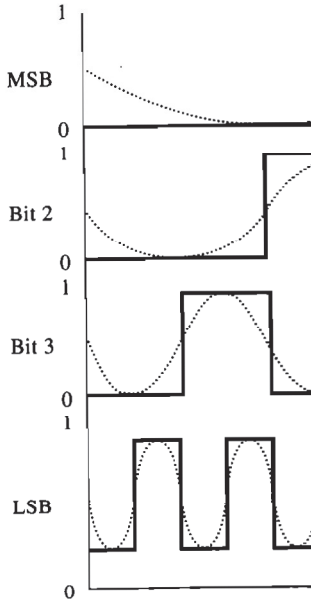

Figure 7.19 The optical trans
each bit channel of the A-to-

to-digital converter, assum
discriminators. The optical
curve, while the correspon

The speed of this A-
the electro-optic switches
tremely fast.

PROBLEMS

7-1 A certain electro-opti
trodes is capable of a
10^{-4} when the maxi
effective index is 3.4
channel waveguide r
on

a. A Mach–Zehnde
b. A coupler switch
waveguides is 1 c

Use the analysis
one waveguide has e